paper in SPIE Proceedings, v. 3875, Materials and Device Characterization in Micromaching, Santa Clara, CA Sept. 1999

A small area in-situ MEMS test structure to measure fracture strength by electrostatic probing

Maarten P. de Boer*, Brian D. Jensen* and Fernando Bitsie**
*Dept. 1725, Intelligent Micromaching
**Dept. 2643, Electromechanical Engineering
Sandia National Laboratories, Albuquerque, NM 87185

http://www.mdl.sandia.gov/Micromachine

ABSTRACT

We have designed, fabricated, tested and modeled a first generation small area test structure for MEMS fracture studies by electrostatic rather than mechanical probing. Because of its small area, this device has potential applications as a lot monitor of strength or fatigue of the MEMS structural material. By matching deflection versus applied voltage data to a 3-D model of the test structure, we develop high confidence that the local stresses achieved in the gage section are greater than 1 GPa. Brittle failure of the polycrystalline silicon was observed.

1. INTRODUCTION

Fracture and fatigue strength is an important criterion in mechanical engineering design. In Microelectromechanical Systems (MEMS), the structural material is often a polycrystalline silicon (polysilicon) thin film, but other thin film materials such as aluminum, amorphous diamond, polycrystalline diamond, and gallium arsenide have been developed or are being considered for future applications. Fracture strength of the thin film can conceivably vary with each manufacturing lot due to potential differences in grain size control or flaw size in the resulting films. In this work we investigate a small area fracture test structure suitable for lot monitoring by electrostatic probing.

For our purposes, the fracture test structure for *process monitoring* should ...
1) be fabricated according to the standard process flow and be tested on-chip without special handling.
2) require only a small area on the chip so that the majority of the real estate can be devoted to the MEMS device.
3) use electrostatics to provide force, as this is the means of actuation in MEMS. The stucture can then be tested simultaneously with other structures which yield information on mechanical and surface properties [1-6] within the framework of the Interferometry for Materials Properties (IMaP) test methodology we are developing.
4) allow verifiable deflections to be measured so that the fracture/fatigue strength can be known to high confidence.
5) be independent of the structural material so that multiple structural materials can be compared.

A multitude of techniques have been proposed to measure fracture strength for MEMS, none of which satisfies sufficiently the criteria above. One common method is to apply a force to a cantilever beam, either by means of a calibrated force probe [7,8], or by measuring deflection of the probe [9-11]. However, electrostatics cannot provide sufficient force to fracture such structures. A second method is to build a MEMS gage sample, remove it from the substrate, attach it to a gripper and characterize it by means of a load-displacment curve [12-14]. This method yields accurate gage dependent and stress concentration results, but requires relatively large samples. Also specimen handling is difficult. Gage data can be obtained by means of a test probe directly exerting force on an as-fabricated tensile sample [15]. A third method is to build a notch or stress concentrator into the device. Fracture can then be induced by high levels of residual strain [16,17]. However, in micromachining fabrication processes, such strain is typically undesirable and therefore eliminated by annealing. Alternatively, electrostatic comb drives can provide the force to induce fracture [18,19]. However, a large area comb drive is required because of its low force per unit area efficiency. A resonance technique where the force is provided by an oscillating electric field has also been explored

[20,21]. To date, fracture has only been induced in this case when a natural crack was first created via nanoindentation.

2. CONCEPT, MODELING AND FABRICATION OF THE TEST STRUCTURE

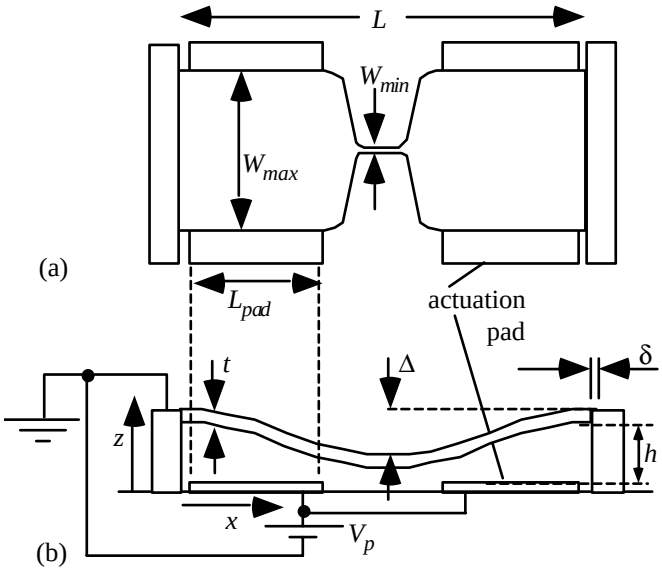

Fig. 1 (a) Top view and (b) side view of the proposed structure

Because of the small forces provided by electrostatics, it is important that a large fraction of the device volume be dedicated to electrostatic force application. Second, a device geometry which creates force and stress amplification is required. A structure which satisfies both of these requirements is shown in Fig. 1. Referring to Fig. 1(b), potential V_p applied across most of the length of the device results in a volume-efficent application of force in the z-direction, with a substational out-of-plane deflection Δ. Because of beam stretching, the force is strongly amplified in the x-direction, as can be shown from beam mechanics. Because force transmitted across the length of the beam must remain constant, stress in the wide portion of the beam is greatly amplified in the thin gage section of Fig. 1(a). From first order beam mechanics, the stress in the ligament is

$$\sigma_{lig} = E\varepsilon_{lig} = E\frac{W_{\max}}{W_{\min}}\left[\frac{1}{2}\left(\frac{\Delta}{L}\right)^2 + \varepsilon_R - 2\frac{\delta}{L}\right] \qquad (1)$$

Here, E is Young's modulus of the beam, W_{max}, W_{min} and L are as in Fig. 1(a), and ε_R is the residual strain in the film. The maximum z-deflection Δ and the deflection δ due to boundary compliance are as shown in Fig. 1(b). From Eq. (1), we see that in order to maximize stress, the ratios $(\Delta/L)^2$ and (W_{max}/W_{min}) should be large, and the deflection δ due to boundary compliance should be minimized. Although it is desirable to have a large residual strain ε_R, this property is usually in the range of a few microstrain in order to be compatible with micromachining device components.

Given that ε_R is typically small, the strongest factor in Eq. (1) is the ratio $(\Delta/L)^2$. We would like to increase Δ in a stable controllable fashion until fracture occurs. A well-known problem in obtaining stable values of Δ while increasing voltage V_p is that beyond a certain pull-in voltage V_{pi}, electrostatic forces exceed restoring forces in the beam. To first order this occurs for $\Delta \sim (h/3)$, where height of the beam h is as shown in Fig. 1(b) [22]. However, the stable range for Δ can be increased significantly by placing the actuation pad only near the support posts at the expense of increasing voltage [23].

With these guidelines in mind, we conducted a parametric study using an approximate two-dimensional finite difference beam model in order to optimize the parameters of Fig. 1 for the test structure. In this study, we assumed $\sigma_R = E\varepsilon_R = 3$ MPa, indicative of our usual polysilicon film (poly) residual stress σ_R of the first level poly (MMPOLY2) in the Sandia National Laboratories SUMMiT micromachining process [24]. A maximum voltage $V_{pad}=V_{max}=200$V applied to the pad was assumed in the model (a conservative value to avoid dielectric breakdown of the air dielectric). We found that using our upper level of polysilicon with h=6 μm (the MMpoly3 layer), significant stresses could develop with this test structure, because then a large stable value of Δ can be obtained. With E=170 GPa, t=2.25 μm, h=6 μm, L=360 μm, L_{pad}=150 μm V_p=200V, σ_R=3 MPa, (W_{max}/W_{min})=200 and ignoring support post deflection δ, the structure was optimized to allow Δ=4.4 μm. Eq. (1) then indicates that a stress σ_{lig}=3.3 GPa can be developed. Making a correction for 2δ=15 nm (as found from subsequent modeling), it appears that it is possible to create a stress σ_{lig}=1.7 GPa. This compares to fracture stress values of σ_f ~1-4 GPa typically observed in the

literature for polysilicon [9,15,25], suggesting that the test structure can indeed be caused to fracture using this approach.

Although refinement of the two-dimensional modeling by resorting to three-dimensional analysis might lead to a better idea for the maximum value possible of σ_{lig}, the maximum voltage V_{max} that could be applied before dielectric breakdown, as well as the stress of the MMPoly3 level σ_R were not well known. Therefore, we decided to layout and fabricate the test structures in order to measure these parameters. In the layout, an attempt was made to maximize the support post rigidity by designing sacrificial oxide cuts with minimum width. Due to the conformal nature of the polysilicon, the support post is a 6 μm solid block of polysilicon throughout its thickness. Details of the support post construction can be found in this proceedings volume (pad 3 in ref. [25]).

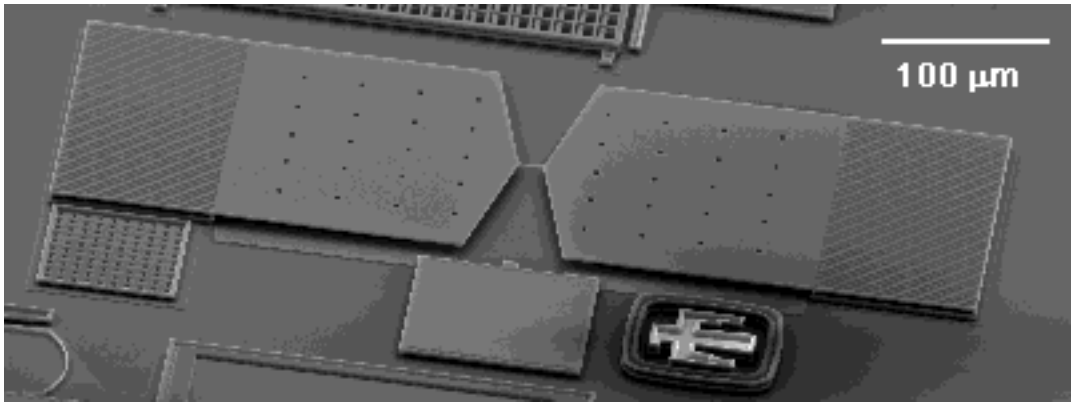

Fig. 2 SEM of a completed device with a 1 μm wide gage section ("Device #2")

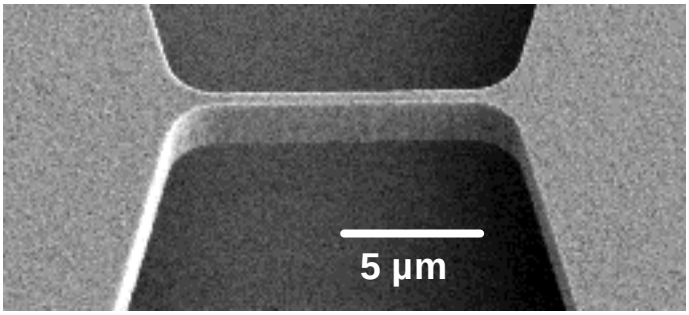

Fig. 3 SEM closeup of the 1 μm gage section test structure ("Device #2") after fabrication and release

The devices were processed according to the SUMMiT process flow [24]. An SEM of the completed device after release is seen in Fig. 2. The layout area including the support post pads on the ends is 200 μm X 500 μm, with an additional pad of 100 μm X 100 μm on the bottom side for pad actuation. Release holes are seen in the portion of the beam which is suspended above the substrate. These are required to ensure that the oxide is entirely removed from under the beam. Gage sections of 10 and 1 micron were studied, and we shall refer to these as "Device 1" and "Device 2" respectively. The structure shown in Fig. 2 has a gage section of 1 μm width. A closeup of the 1 micron gage section is shown in Fig. 3.

3. IN-SITU INTERFEROMETRY OF TEST STRUCTURE ACTUATION

We describe initial test results for the two devices. The devices were electrostatically probed in air while being imaged under interferometric conditions by use of a Michelson attachment on a 10X objective lense. The test setup is as described in ref. [2], and allows measurement of the beam deflections to approximately 10 nm accuracy. Voltage was supplied by a Keithly 487 picoammeter, capable of 500V output. We verified that its voltage output increases smoothly when voltage is increased (i.e. no voltage spikes) by means of a storage oscilloscope. Current was simultaneously measured.

An example interferometric image of an actuated device is shown in Fig. 4. Here, a voltage V_p=215V is applied, inducing significant deflections, similar to Fig. 1(b). Background fringes are aligned parallel to the length of the device, so that fringes along the length of the beam indicate out-of-plane (z) deflections. Each fringe represents a deflection $\lambda/2$=275 nm for the monochromatic green light used. From a digitized linescan, the fringes are

interpreted to obtain point by point *z*-deflections with a resolution of ~1.25 μm in *x*. Deflection curves (through the center line of the structure) vs. actuation voltage for Device #1 are seen in Fig. 5.

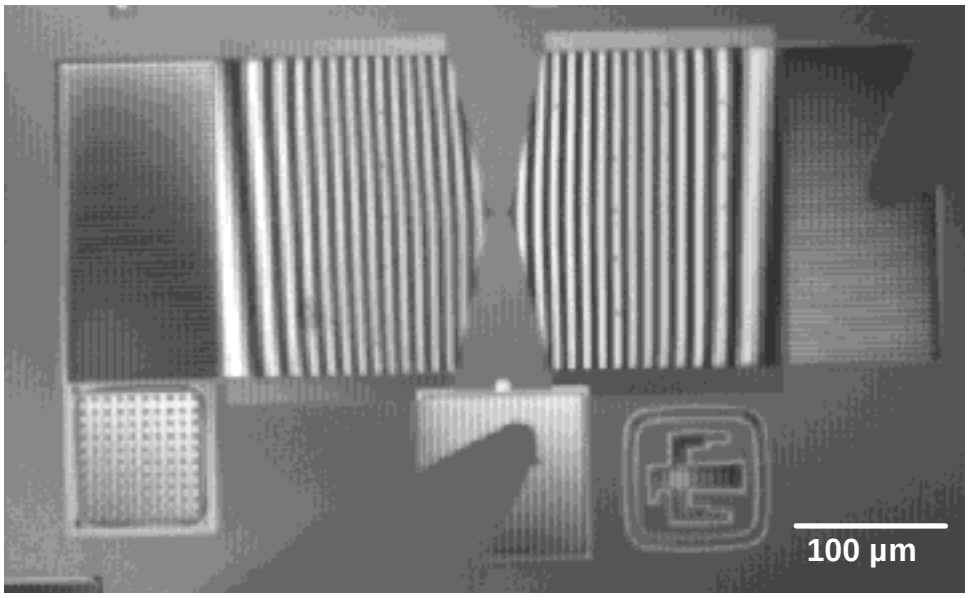

Fig. 4 Interferogram of Device #2 (1 μm wide gage section). The device is stably pulled in to ²=3.9 μm with Vp=215V.

As the voltage is increased, high stress levels are developed in the gage section, and the desired outcome is that the gage section will fracture. Then, knowing the deflections just before fracture, a well-known fracture stress can in principle be calculated. However, besides fracture, two undesired effects may result. The first is electrostatic breakdown of the air dielectric, and the second is device pull-in.

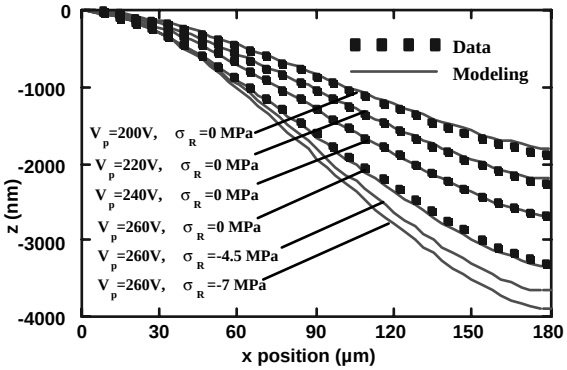

Fig. 5 Experimental vs. modeled deflections for Device #1 (10 μm wide gage section)

We first discuss the electrostatic breakdown voltage, V_{EBD}. Device #1 is significantly stiffer than Device #2, and could repeatably sustain a voltage of up to 260 volts. According to ref. [26], when electrostatic breakdown initiates, the actuator shows chaotic fluctuations. At V_p=260V, no such behavior was observed, nor did the deflections reduce over time as would be the case if discharge events had occurred. Current in the nanoampere regime flowed at V_p>260V. We believe that this was due to surface conduction between the actuation pad and the grounded beam rather than due to electrostatic breakdown. Pull-in was observed at 265-270V for Device #1. We conclude that electrostatic breakdown voltage V_{EBD} is at least 270V. This is in agreeement with the literature on this topic: Paschen curves exhibit a sharp increase in breakdown voltage below a 10 micron gap size [27]. When pull-in occurred at 260-270V, the gage section in Device #1 did not fracture. Current did increase because of beam contact with the underlying actuation pad, and damage to the actuation pad at the point of contact did occur.

A catastrophic event for Device #2 occurred at V_p values of 150, 211, 213 and 218 volts, resulting in a gage section separation. Because V_{EBD}>270V, the event must signify either fracture or pull-in. It is currently difficult to distinguish experimentally between these phenomena. In the next section, we apply three-dimensional simulation in order to determine which of these events likely occurred. If the simulation indicates the pull-in voltage is greater than 220V, fracture likely occurred. Otherwise pull-in and subsequent fracture occurred. In the case of pull-in first, we can report a minimum stress level that the polysilicon can exceed.

4. THREE DIMENSIONAL MODELING

In order to determine if the catastrophic event for Device #2 for V_p between 210 and 220V volts was due to fracture or pull-in, we created a three-dimensional finite element model with a coupled solution between the electrostatics and the mechanical structure. First, Device #1 was modeled, and the modeled deflection results are compared to the

measured data in Fig. 5. In order to obtain this agreement, the parameters of Fig. 1 including h=6.62 μm, t=2.28 μm were measured, the residual stress in the beam σ_R was varied from 0 to –7 MPa, and the compliance of the boundaries was modeled with a simple short cantilever beam approximation similar to ref. [28]. We see in Fig. 5 that at σ_R =0 MPa, the deflections are well matched at a series of voltages V_p from 200 to 260V. To show the resolution with respect to σ_R, the deflections at V_p=260V are also shown with σ_R =-4.5 and –7.0 MPa. Clearly the best agreement is at σ_R =0 MPa. With σ_R =0, the pull-in voltage was found to be 265V, in good agreement with our experimental data of 260-270V.

Next we modeled Device #2, using the same parameters as above. We found that assuming a gage section of 1 micron, there were systematic differences between the measured and modeled deflections. The actual linewidth of the gage section was measured by SEM, and found to be 0.78 μm. We are in the process of improving the agreement between the measured and modeled data for Device #2. Thus far, we have seen that the model is very sensitive to the value of the gage section linewidth. It appears that the pull-in voltage is approximately 215V, very close to the measured values.

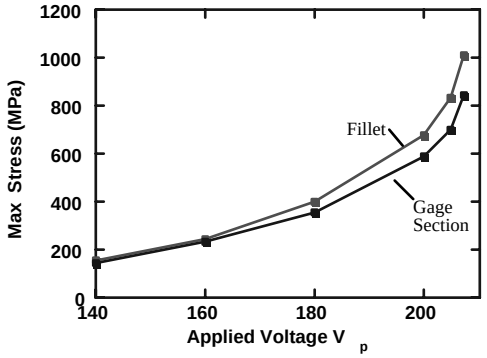

Fig. 6 Max principle stresses in a 0.7 μm gage section and the fillet vs. V_p.

Independent of whether the catastrophic event is due to pull-in or fracture, we can place a lower bound on the stress which the material can withstand. The maximum principal stresses in the gage section and fillet as a function of actuation voltage V_p are as shown in Fig. 6. In this simulation, the maximum stress occurs in the fillet area, which has a radius of curvature of 2 microns. Simulations have shown that with a 4 μm radius of curvature, the stress is maximized in the gage section rather than in the fillet. The maximum stress along the bottom of the gage section is nearly uniform, indicating that the curvature of the beam is constant.

5. FAILURE ANALYSIS

Examples of the fractography of Device #2 are shown in the SEMs of Figs. 7 and 8. For the sample which failed at 150V, a clear brittle fracture signature is observed in Fig. 7. However, the failure for the other samples was as in Fig. 8. Here we see that the ligament area itself has undergone melting. Further, there is damage to the underlying nitride. Similar damage was seen on the other side of the ligament. Apparently after fracture and separation from

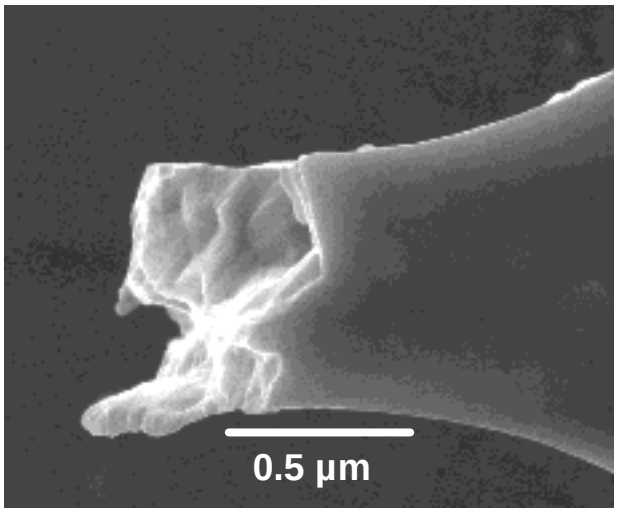

Fig. 7 Example of intergranular fracture in Device #2 (1 μm gage section) for Vp=150V.

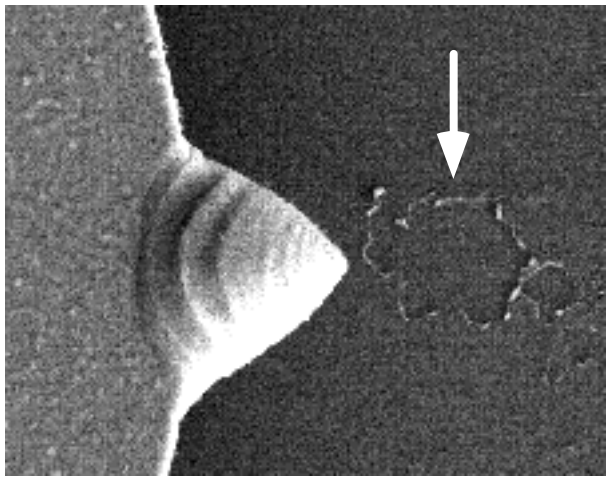

Fig. 8 SEM view of failed Device #2 (1 μm ligament). Arrrows indicates area where underlying nitride shows electrostatic damage.

the voltage supply, sufficient charge remains in the newly created cantilever beam to cause the underlying nitride to fail by electrostatic breakdown. When this occurs, a large current flows through the ligament, and it vaporizes. This problem can be avoided by designing a ground plane poly layer electrically connected to the fixed fixed beams. Fractography should then be possible for all the failed samples.

6. SUMMARY AND CONCLUSIONS

Using the principles of force and stress amplification, we designed an electrically probeable MEMS fracture test structure which achieves ~1 GPa level principle stresses in the gage section, while occupying an area of only ~0.01 mm^2. This test structure is useful for establishing a lower bound for stresses in polysilicon, and can be useful for fatigue studies in non-brittle materials. Testing of a 10 μm wide gage section test structure indicates that the electrostatic breakdown voltage in air is greater than 270 volts. Both experimental evidence and 3-D electrostatic simulations of the deflections indicate that the 10 μm gage section structure fails by electrostatic pull-in. After pull-in, the 10 μm gage section remains intact. For a 1 μm wide gage section test structure, gage section failure occurs over a range of voltages from 150-218V. A lower bound for the fracture strength of the test structures is ~ 1 GPa.

With optimization of the test structure with 3-D modeling, we will be able to move the maximum stress region into the gage section. Also, increased stresses before pull-in may be possible. A poly pad on the substrate under the gage section with electrically connection to the beam structure will allow improved fractography for this device.

These improvements will the enable this test structure to be used as a fracture/fatigue for high volume process monitoring in conjunction with other test structures we are developing. These include devices to monitor strain gradient, mechanical properties such as Young's modulus and residual stress, support post compliance, adhesion, adhesion hysteresis, friction and wear [1-6].

7. ACKNOWLEDGMENTS

We thank the staff at the Microelectronics Development Laboratory for fabricating and releasing the samples in this work, Daniel Gutierrez for testing the samples, and Bonnie McKenzie for the SEM images. Sandia is a multiprogram laboratory operated by Sandia Corporation, a Lockheed Martin Company, for the United States Department of Energy under Contract DE-AC04-94AL85000.

8. REFERENCES

[1] B. D. Jensen, M. P. de Boer and S. L. Miller, "*IMaP: Interferometry for materials property evaluation in MEMS*," presented at MSM '99, San Juan, Puerto Rico, 1999, pp. 206-209.

[2] M. P. de Boer, M. R. Tabbara, M. T. Dugger, P. J. Clews and T. A. Michalske, "*Measuring and modeling electrostatic adhesion in micromachines*," presented at Transducers '97, Chicago, IL, USA, 1997, pp. 229-232.

[3] M. P. de Boer, J. M. Redmond and T. A. Michalske, "*A hinged-pad test structure for sliding friction measurement in micromachinig*," presented at SPIE, Santa Clara, CA, 1998, pp. 241-250.

[4] M. P. de Boer and T. A. Michalske, "*Accurate method for determining adhesion of cantilever beams*," J. Appl. Phys. **86** (2), 15 July (1999).

[5] M. P. de Boer, P. J. Clews, B. K. Smith and T. A. Michalske, "*Adhesion of polysilicon microbeams in controlled humidity ambients*," Mater. Res. Soc. Proc. **518**, 131 (1998).

[6] M. P. de Boer, T. M. Mayer, T. A. Michalske, U. Srinivasan and R. Maboudian, "*Adhesion performance of silane coupling agents at high humidity levels*," Langmuir, **to be submitted** (1999).

[7] T. P. Weihs, S. Hong, J. C. Bravman and W. D. Nix, "*Mechanical deflection of cantilever microbeams: a new technique for testing the mechanical properties of thin-films*," J. Mater. Res. **3**, 931 (1988).

[8] F. Ericson and J-A. Schweitz, "*Micromechanical fracture strength of silicon*," J. Appl. Phys. **68**, 5840 (1990).

[9] C. J. Wilson, A. Ormeggi and M. Narbutovskih, "*Fracture testing of silicon microcantilever beams*," J. Appl. Phys. **79** (5), 2386 (1996).

[10] P. T. Jones, G. C. Johnson and R. T. Howe, "*Fracture strength of polycrystalline silicon*," Mater. Res. Soc. Proc. **518**, 197 (1998).

[11] S. C. Bromley, L. L. Howell and B. D. Jensen, "*Determination of maximum allowable strain for polysilicon micro-devices*," Eng. Fail. Anal. **6**, 27 (1999).
[12] D. T. Read and J. W. Dally, "*A new method for measuring the strength and ductility of thin-films*," J. Mater. Res. **8** (7), 1542 (1993).
[13] W. N. Sharpe, B. Yuan and R. L. Edwards, "*A new technique for measuring the mechanical properties of thin-films*," J. Microelectromech. Syst. **6** (3), 193 (1997).
[14] W. Suwito, M. L. Dunn, S. H. Cunningham and D. T. Read, "*Elastic moduli, strength and fracture initiation at sharp notches in etched single crystal silicon microstructures*," J. Appl. Phys. **85** (7), 3519 (1999).
[15] S. Greek, F. Ericson, S. Johansson and J-A. Schweitz, "*In-situ tensile strength measurement and weibull analysis of thick-film and thin-film micromachined polysilicon structures*," Thin Solid Films **292** (1-2), 247 (1997).
[16] L. S. Fan, R. T. Howe and R. S. Muller, "*Fracture toughness characterization of brittle thin films*," Sensors and Actuators A **A21-A23**, 872 (1990).
[17] M. Biebl and H. von Philipsborn, "*Fracture strength of doped and undoped polysilicon*," Proc. Int. Conf. Solid-State Sensors & Actuators (Transducers '95) , 72 (1995).
[18] R. Ballarini, R. L. Mullen, Y. Yin, H. Kahn, S. Stemmer and A. H. Heuer, "*The fracture toughness of polysilicon microdevices - a first report*," J. Mat. Res. (1997).
[19] M. T. A. Saif and N. C. MacDonald, "*Microinstruments for submicron materials studies*," J. Mater. Res. **13** (12), 3353 (1998).
[20] J. A. Connally and S. B. Brown, "*Slow crack-growth in single crystal silicon*," Science **256** (5063), 1537 (1992).
[21] S. B. Brown, W. Van Arsdell and C. L. Muhlstein, "*Materials reliability in MEMS devices*," Proc. Int. Conf. Solid-State Sensors & Actuators (Transducers '97) **1**, 591 (1997).
[22] P. Osterberg, H. Yie, X. Cai, J. White and S. Senturia, "*Self-consistent simulation and modeling of electrostatically deformed diaphragams*," presented at IEEE '94, 1994, pp. 28-32.
[23] E. S. Hung and S. D. Senturia, "*Leveraged bending for full-gap positioning with electrostatic actuation*," presented at Hilton Head '98, Hilton Head Island, SC, USA, 1998, pp. 83-86.
[24] J. J. Sniegowski, "*Multi-level polysilicon surface-micromachining technology: applications and issues*," presented at ASME IMECE, Atlanta, GA, Nov. 1996, 1996, pp. 751-759.
[25] B. D. Jensen, M. P. de Boer and F. Bitsie, "*Interferometric measurement for improved understanding of boundary effects in micromachined beams*," this proceedings (1999).
[26] J. Wibbeler, G. Pfeifer and M. Hietschold, "*Parasitic charging of dielectric surfaces in capacitive microelectromechanical systems (MEMS)*," Sensors and Actuators A **A71**, 74 (1998).
[27] M. Madou, *Fundamentals of Microfabrication* (CRC Press, Boca Raton, Florida, 1997).
[28] Q. Meng, M. Mehregany and R. L. Mullen, "*Theoretical modeling of microfabricated beams with elastically restrained supports*," J. Microelectromech. Syst. **2** (3), 128 (1993).